GLOBAL BIOGEOCHEMICAL CYCLES, VOL. 23, GB4015, doi:10.1029/2009GB003472, 2009

North Atlantic production of nitrous oxide in the context of changing atmospheric levels

A. Freing,[1] D. W. R. Wallace,[1] T. Tanhua,[1] S. Walter,[1,2] and H. W. Bange[1]

Received 16 January 2009; revised 25 May 2009; accepted 7 July 2009; published 3 November 2009.

[1] We use transit time distributions calculated from tracer data together with in situ measurements of N_2O to estimate the concentration of biologically produced N_2O ($[N_2O]_{xs}$) and N_2O production rates in the central North Atlantic Ocean. Our approach to estimation of N_2O production rates integrates the effects of potentially varying production and decomposition mechanisms along the transport path of a water mass. We find that previously used approaches overestimate the oceanic equilibrium N_2O concentrations by 8–13% and thus underestimate the strength of N_2O sources in large parts of the water column. Thus the quantitative characteristics of the $[N_2O]_{xs}$/AOU relationship used as an indicator of nitrification are distorted. We developed a new parameterization of N_2O production during nitrification depending linearly on AOU and exponentially on temperature and depth, which can be applied to calculate N_2O production due to nitrification in the entire ocean including oxygen minimum zones.

Citation: Freing, A., D. W. R. Wallace, T. Tanhua, S. Walter, and H. W. Bange (2009), North Atlantic production of nitrous oxide in the context of changing atmospheric levels, *Global Biogeochem. Cycles*, *23*, GB4015, doi:10.1029/2009GB003472.

1. Introduction

[2] Nitrous oxide (N_2O) is an important atmospheric trace gas, which influences, directly and indirectly, the Earth's climate: In the troposphere it acts as a greenhouse gas, and in the stratosphere it is the major source for nitric oxide radicals, which are involved in one of the main ozone reaction cycles [*IPCC*, 2007]. The global warming potential of N_2O on a 100-year basis equals 298 times the global warming potential of CO_2 [*IPCC*, 2007]. Since the beginning of the industrial revolution the global mean tropospheric N_2O mole fraction has risen rapidly from 275 ppb up to 319 ppb in 2005 [*IPCC*, 2007]. One of the main natural sources of atmospheric N_2O is microbial nitrous oxide production in the ocean [*IPCC*, 2007].

[3] In the ocean, the excess of N_2O over the atmosphere equilibrium concentration ($[N_2O]_{xs}$) is a measure to diagnose the production of N_2O in different water masses [*Nevison et al.*, 1995, 2003]. It is defined as

$$[N_2O]_{xs} = [N_2O]_{insitu} - [N_2O]_{eq}, \quad (1)$$

where $[N_2O]_{insitu}$ is the in situ concentration of N_2O and $[N_2O]_{eq}$ is the concentration of N_2O in equilibrium with the atmosphere at the time of the last atmospheric contact.

[4] For the preindustrial ocean and water masses ventilated before 1800,

$$[N_2O]_{eq} = [N_2O]_{eq}^{preind} = X_{N_2O_{preind}} P H_{T,S}, \quad (2)$$

where $X_{N_2O_{preind}}$ is the preindustrial atmospheric mixing ratio of N_2O, P is the atmospheric pressure and $H_{T,S}$ is the temperature-dependent and salinity-dependent solubility of N_2O in seawater [*Weiss and Price*, 1980].

[5] For water masses which were fully or partially ventilated by water originating at the sea surface since 1800, the calculation of $[N_2O]_{eq}$ is more complicated. For these water masses the effect of the anthropogenic increase of the N_2O atmospheric mixing ratio needs to be considered, and an atmospheric mole fraction for the time of the last contact of the water mass with the atmosphere has to be estimated. This implies that the "age" of the water mass has to be determined. However, water masses are generally mixtures of fractions with different origins and, usually, different ages.

[6] In most previous studies used for such calculations [e.g., *Nevison et al.*, 2003; *Butler et al.*, 1989; *Yoshinari*, 1976], the contemporary atmospheric mole fraction has been used, independent of the "real" age of the sampled water masses. This procedure is well suited for calculating N_2O_{xs} for near-surface waters, but ignores the effect of variable water mass age and hence the variable atmospheric mole fraction involved in establishing initial "equilibrium" N_2O concentrations for the deeper layers of the ocean. *Nevison et al.* [2003] acknowledge that the use of only the contemporary atmospheric mole fraction introduces an uncertainty of 10–15% in the estimate of $[N_2O]_{xs}$.

[1]Marine Biogeochemistry Research Division, Leibniz Institute for Marine Sciences, IFM-GEOMAR, Kiel, Germany.
[2]Now at Institute for Marine and Atmospheric Research Utrecht, Utrecht University, Utrecht, Netherlands.

0886-6236/09/2009GB003472$12.00

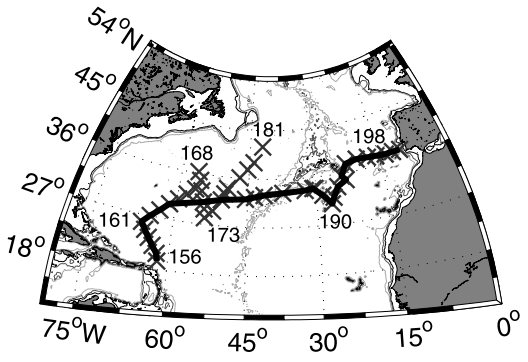

Figure 1. Cruise track of the M60/5 cruise in 2004. The crosses marks individual stations; the stations used for the W-E section in Figure 5 are joined with the solid line. Selected station numbers are indicated.

[7] To address this issue, a water mass age-dependent method to calculate $[N_2O]_{xs}$ was introduced for the first time by *Walter et al.* [2006]. They used three separate atmospheric mole fractions based on roughly estimated water mass ages in order to calculate N_2O equilibrium concentrations. With this approach the calculated equilibrium concentration of N_2O for water masses below the thermocline was lower than calculated using the contemporary N_2O mole fraction.

[8] This paper introduces an improved approach to calculating $[N_2O]_{xs}$ by using transit time distributions (TTD) for water samples in which N_2O was measured. The TTD concept allows an age distribution to be estimated for a sampled water mass on the basis of measurements of transient tracers such as CFCs [*Waugh et al.*, 2003]. TTDs make it possible to estimate relative age distributions of a water mass which can then be applied to calculate an effective value for $[N_2O]_{eq}$. Moreover, the calculated age provides means to calculate in situ nitrous oxide production rates.

2. Methods

2.1. Study Area

[9] The data presented here were collected in the midlatitude North Atlantic Ocean during spring 2004 on board the German research vessel R/V Meteor [*Tanhua et al.*, 2006; *Walter et al.*, 2006]. The cruise track of the Meteor cruise 60/5 was from Martinique to Lisbon, with a northernmost station at 42°N, 42°W, and the cruise therefore included sampling of both the subtropical and cold-temperate gyre, as well as the western and eastern basins (see Figure 1). Most stations were repeat samplings of stations from the Transient Tracers in the Ocean Program (TTO-NAS) in 1982.

2.2. N_2O, SF_6, and CFC Measurements

[10] Water samples for N_2O analysis were collected at 37 stations in triplicate from various depths, taken with a 24-Niskin-bottle rosette, equipped with a CTD-sensor. Samples were then analyzed gas-chromatographically using an electron capture detector. The analytical method applied for N_2O analysis is described in detail by *Walter et al.* [2006]. For the two-point calibration procedure we used standard gas mixtures with 311.8 ± 0.2 ppb and 346.5 ± 0.2 ppb N_2O in synthetic air, which have been calibrated against the National Oceanic and Atmospheric Administration (NOAA, Boulder, Colorado) standard scale in the laboratories of the Air Chemistry Division of the Max-Planck Institute for Chemistry, Mainz, Germany. The overall relative mean analytical error is estimated to be ±1.8%.

[11] N_2O concentrations are denoted by brackets and are generally reported in nmol kg^{-1}. All measured profiles are displayed in Figure 2.

[12] The determination of SF_6 was performed by purge-and-trap gas chromatography with electron capture detection [*Tanhua et al.*, 2005]. The analytical precision was ±1.5%, the detection limit was estimated to be 0.05 fmol kg^{-1} (∼0.15 ppt), and a sampling blank (determined from analyses of deep water samples in the eastern basin) of the same magnitude has been subtracted from the data. The SF_6 data were calibrated against an air standard prepared at CMDL, Boulder, Colorado, and recalibrated to the GMD2000 scale (http://www.cmdl.noaa.gov/hats/standard/SF6_scale.htm).

[13] The CFC measurements were made on an analytical system similar to that described by *Bullister and Weiss* [1988] and are reported on the SIO98 scale [*Prinn et al.*,

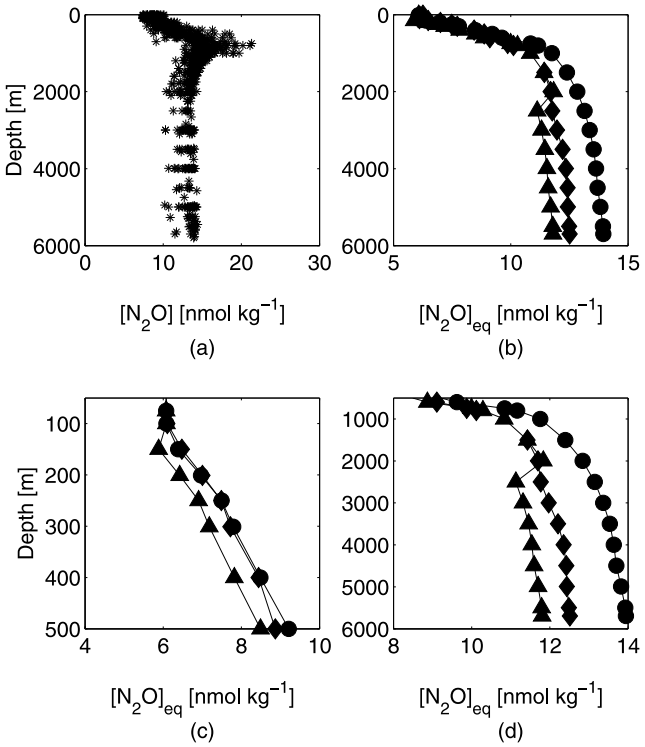

Figure 2. (a) In situ N_2O concentrations (nmol kg^{-1}) versus depth (m). (b) Comparison of profiles at station 156 of $[N_2O]_{eq}$ (nmol kg^{-1}) versus depth (m) for the three different approaches ("contemporary," denoted by circles, "layer," denoted by triangles, and "TTD," denoted by diamonds). (c) The 0–500 m section of Figure 2b. (d) The 500–2500 m section of Figure 2b.

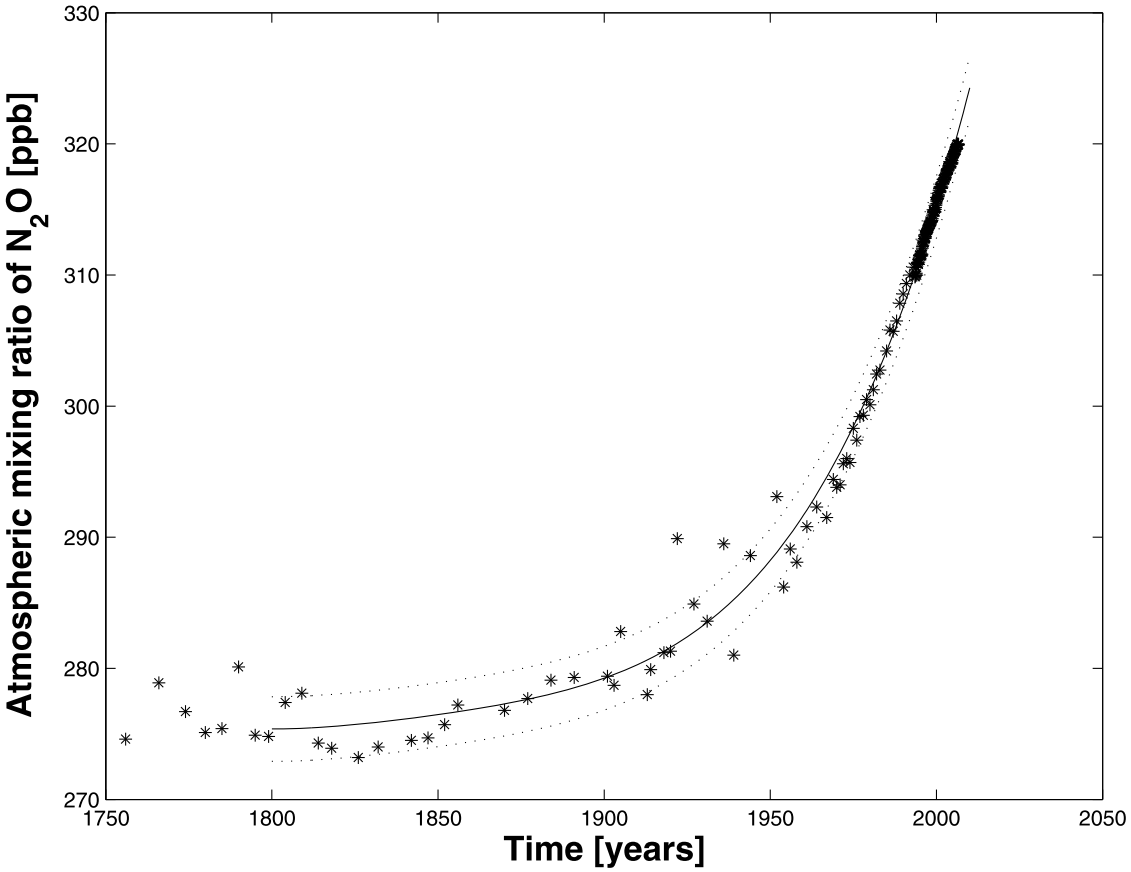

Figure 3. The in situ air measurements, firn measurements, and ice-core data we used for reconstructing the atmospheric history of N_2O [*Machida et al.*, 1995; *Battle et al.*, 1996]. The best fit we used for the analysis (see equation (3)) is shown as a black line; the dotted lines represent 95% confidence intervals for an individual observation.

2000]. The analytical precision was 0.7% for CFC-12, and a sampling blank of 0.007 pmol kg^{-1} (determined as the median value of 18 deep water samples in the eastern basin) has been subtracted from the data.

[14] The salinity-dependent and temperature-dependent solubility of CFC-12, SF_6, and N_2O are calculated from their respective solubilities [*Bullister et al.*, 2002; *Warner and Weiss*, 1985; *Weiss and Price*, 1980], and we have assumed an atmospheric pressure of 1 atmosphere over the surveyed area. In this way, tracer concentrations can be compared directly to the time-varying atmospheric histories of these compounds [*Maiss and Brenninkmeijer*, 1998; *Walker et al.*, 2000].

2.3. Atmospheric History of N_2O

[15] In order to estimate the background N_2O signal in the ocean we need to know the time-dependent history of atmospheric concentrations. For this work, we have used a synthesis of ice-core and firn data [*Machida et al.*, 1995; *Battle et al.*, 1996] merged with air measurements. The data are available at http://daac.ornl.gov [*Holland et al.*, 2005]. We assumed a constant atmospheric mixing ratio of N_2O of 275 ppb prior to year 1800 and used a polynomial fit of the data (Figure 3) from 1800 to the present day. The atmospheric mixing ratio of N_2O ($X_{N_2}O$) in nmol mol^{-1} was calculated as

$$X_{N_2O}(t) = -0.0004t^3 + 1.0520t^2 - 1288.6261t + 592247.9514, \quad (3)$$

where t denotes the sampling year, $1800 < t < 2008$.

2.4. Transit Time Distributions

[16] Following *Waugh et al.* [2003], it is assumed that the age distribution (TTD) of a water parcel, produced by different transport pathways and mixing, can be described as an inverse Gaussian function.

[17] Since this function is a Green's function, it can be used to calculate the concentration c of a conservative tracer at any given point in space r and any given time t:

$$C(r,t) = \int_0^\infty c_0(t-t')G(r,t')dt', \quad (4)$$

where c_0 is the input function of the tracer at the sea surface and $G(r, t')$ is the TTD.

[18] To uniquely determine an inverse Gaussian age distribution, one needs to determine its two parameters Γ, the mean age, and Δ, the width of the distribution. In order to estimate these from observations of a single transient tracer, such as CFC-12 or SF_6, one needs to make an assumption about the ratio of Γ and Δ.

[19] *Waugh et al.* [2004] showed that a ratio of $\Gamma/\Delta = 1$ is consistent with the distribution of a range of different tracers, and *Tanhua et al.* [2008] confirmed that this value is appropriate for the midlatitude North Atlantic Ocean from the M60/5 cruise.

[20] The TTD is then given by

$$G(t) = \sqrt{\frac{\Gamma^3}{\pi 4\Delta^2 t^3}}\ \exp\left(\frac{-\Gamma(t-\Gamma)^2}{4\Delta^2 t}\right), \tag{5}$$

2.5. Calculation of Excess N_2O

[21] Three different approaches have been used to calculate $[N_2O]_{eq}$ and hence $[N_2O]_{xs}$.

[22] 1. The "contemporary" approach: $[N_2O]_{eq}$ was calculated based on the contemporary atmospheric dry mole fraction of N_2O [e.g., *Nevison et al.*, 2003; *Butler et al.*, 1989; *Yoshinari*, 1976]. The problem is that the "contemporary" atmospheric dry mole fraction of N_2O has increased every year since 1800.

[23] 2. The "layer" approach used by *Walter et al.* [2006]: Given that equilibration time for N_2O between the ocean surface layer and the atmosphere is fast (3 weeks) relative to the atmospheric growth rate [*Najjar*, 1992], $[N_2O]_{eq}^{layer}$ in the mixed layer was calculated using the contemporary atmospheric N_2O value (319 ppb for the year 2005) [*IPCC*, 2007]. For depths greater than 2000 m, $[N_2O]_{eq}^{layer}$ was calculated using the tropospheric preindustrial value of 270 ppb [*Flückinger et al.*, 1999] as, generally, tropical Atlantic deep waters below 2000 m are older than 200 years [*Broecker and Peng*, 2000].

[24] For the depth range between the upper thermocline and 2000 m an average of the actual and the preindustrial atmospheric value was used (294 nmol mol^{-1}). Hence:

$$[N_2O]_{eq}^{layer} = \begin{cases} 319\ H_{T,S}\ P & \text{for mixed layer samples} \\ 294\ H_{T,S}\ P & \text{for samples between thermocline and 2000 m} \\ 270\ H_{T,S}\ P & \text{for samples deeper than 2000 m} \end{cases} \tag{6}$$

where $H_{T,S}$ is the solubility of N_2O in seawater [*Weiss and Price*, 1980] and P is the atmospheric pressure.

[25] 3. The "TTD" approach introduced here: CFC-12 and SF_6 data from the M60/5 cruise were used to calculate the transit time distribution, the TTD. *Tanhua et al.* [2008] have shown that use of SF_6 results in a more reliable estimation of TTDs for younger water masses. Hence SF_6 data (if available) were used for samples from "younger" water masses, and CFC-12 data were used for all other samples, where "young waters" are defined as having CFC-12 values larger than 450 pmol mol^{-1}.

[26] The equilibrium N_2O concentration was then calculated as the integral of the different fractions multiplied by their respective equilibrium concentrations, where the atmospheric mixing ratios were calculated using the sampling year and the polynomial fit as described in equation (3).

$$[N_2O]_{eq}^{TTD}(t) = \int_0^\infty H_{T,S}\ X_{N_2O}(t-t')\ G(t')\ dt', \tag{7}$$

where t is the sampling year, $H_{T,S}$ is the solubility of N_2O in seawater [*Weiss and Price*, 1980], $X_{N_2}O$ is the atmospheric history of N_2O (see equation (3)), and G is the calculated transit time distribution (see equation (5)).

[27] The 95% confidence intervals for an individual observation associated with the atmospheric history used for the "TTD" approach are indicated in Figure 3. Within these bounds the fitted values differ by less than 2.5 ppb from the extreme observations. A difference of 2.5 ppb leads to a difference in $[N_2O]_{eq}$ and $[N_2O]_{xs}$, respectively, of 0.06–0.1 nmol kg^{-1} for a range of suitable temperatures.

[28] This calculation of N_2OPR is based on the assumption that N_2O starts off at equilibrium with the atmosphere, which is not necessarily true for every water mass. *Körtzinger et al.* [2004] observed, however, that O_2, where unaffected by biology, was uniformly distributed at close-to-equilibrium concentrations even within an extremely deep winter-mixed layer (1400 m) in the Labrador Sea. As N_2O displays similar solubility characteristics as O_2 it is likely to be the same for N_2O. An undersaturation/supersaturation of 2% has approximately the same quantitative effect on $[N_2O]_{eq}$ as has the uncertainty of the atmospheric history.

[29] Additionally, it is assumed that $[N_2O]_{xs}$ is not significantly altered by mixing of water with different temperatures, salinities and hence N_2O solubilities. The uncertainty thus introduced only attains the range of the uncertainty introduced by the atmospheric history ($\sim$0.1 nmol kg^{-1}) if water masses differing by 5°–10°C in temperature are mixed. Therefore it is negligible.

[30] The results of these three approaches are compared in section 3.1.

2.6. Apparent N_2O Production Rate

[31] An apparent N_2O production rate (N_2OPR) was calculated as

$$N_2OPR = \frac{[N_2O]_{xs}}{\bar{t}}, \tag{8}$$

where $\bar{t}$ is the mean age of the water sample calculated from the sample's TTD.

[32] To exclude any undue influence of short-term seasonal variations affecting the near-surface ocean in the estimated mean age, production rates were only calculated for samples with a mean age of at least 1 year. This explicitly excludes mixed layer samples.

[33] A mean N_2OPR for a water sample based on a history of advection mixing and N_2O production is not necessarily equivalent to a local or instantaneous N_2O

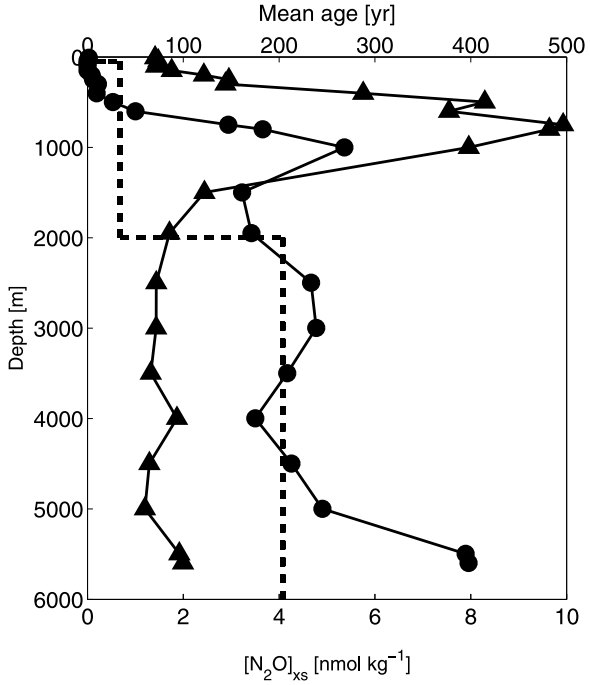

Figure 4. $[N_2O]_{xs}$ in nmol kg^{-1} (denoted by triangles) and mean age according to the "TTD" approach in years (denoted by circles) versus depth in m at station 158. Dashed lines indicate the mean age assumed by the "layer" approach.

production rate. However, scaling by the mean age is a way of averaging the N_2O production and attaching less weight to singular influential events. This means in particular that short-lived features of the N_2O production rate cannot be represented this way but will be averaged out.

2.7. Apparent Oxygen Utilization Rate

[34] The apparent oxygen utilization rate (AOUR) was estimated in a similar fashion:

$$\mathrm{AOUR} = \frac{[\mathrm{AOU}]}{\bar{t}}, \tag{9}$$

where $\bar{t}$ is the mean age of the water sample calculated with the TTD method.

[35] As for N_2O production rates, apparent oxygen utilization rates were only calculated for samples with a mean age of at least 1 year.

3. Results and Discussion

3.1. Comparison of Different Approaches for $[N_2O]_{eq}$ Calculation

[36] The effect of using different approaches to calculate $[N_2O]_{eq}$ is shown in Figure 2. In surface waters, all three methods agree, as all methods employ the contemporary atmospheric N_2O mole fraction to calculate the N_2O background for this layer.

[37] The TTD method is likely to be the quantitatively most appropriate method of calculating $[N_2O]_{eq}$ and $[N_2O]_{xs}$ as it uses a more sophisticated approach to age estimation. However, as noted earlier, the TTD approach still cannot determine where and when the excess N_2O was produced. The measured N_2O concentration represents an integrated estimate of $[N_2O]_{xs}$, which was produced along the transport path and mixing history of the water parcel. Figure 4 shows exemplary profiles of mean age and $[N_2O]_{xs}$ versus depth. The uncertainty introduced by the approach amounts to 0.06–0.1 nmol kg^{-1} for a range of suitable temperatures (see section 2.5).

[38] The "layer" approach uses only three different atmospheric mixing ratios and is therefore a very rough approach to dealing with the atmospheric change displayed in Figure 3. As a result, application of this method produces sharp and unrealistic steps in background N_2O profiles (see Figure 2). In addition, this method also appears to slightly overestimate the age of water masses found below 2000 m in comparison to the TTD approach. This arises from the approach's failure to account for mixing with "younger" waters enriched in N_2O. It is worth noting, that for the "layer" approach the value of 294 ppb used for the intermediate layer differs by 24 ppb for the year 2004. This difference, which will most likely continue to increase due to the changing atmospheric mole fraction, leads to a difference in $[N_2O]_{eq}$ and $[N_2O]_{xs}$, respectively, of 0.5–1.2 nmol kg^{-1} for a range of suitable temperatures.

[39] Figure 2 shows that the commonly used "contemporary" approach systematically overestimates $[N_2O]_{eq}$ by 8–13% and thus underestimates $[N_2O]_{xs}$ below the mixed layer, making it inappropriate for quantitative assessment of N_2O production in deeper parts of the water column. Depending on the actual age of the water mass concerned, the "contemporary" approach can lead to a difference in $[N_2O]_{eq}$ and $[N_2O]_{xs}$ of up to 1–2 nmol kg^{-1} for a range of suitable temperatures.

3.2. Excess N_2O Concentrations

[40] The measured $[N_2O]$ profiles (Figure 2) display a distinct peak around 700–1000 m, which has no equivalent in the $[N_2O]_{eq}$ profiles (Figure 2), and must therefore be the result of in situ production. Figure 5 shows $[N_2O]_{xs}^{TTD}$ along a west to east transect in the midlatitude North Atlantic. In line with the results displayed in Figure 2, maximum values of $[N_2O]_{xs}^{TTD}$ of 6–12 nmol kg^{-1} were found around 700–1000 m indicating that this part of the water column has accumulated a significant amount of N_2O.

[41] The $[N_2O]_{xs}^{TTD}$ peak appears to be slightly shallower and to be more pronounced in the western basin compared to the eastern basin. At shallower depth there is a clear difference in the magnitude of the $[N_2O]_{xs}$ maximum between the eastern and the western basins. Maximum concentrations in the western basin reach up to 12 nmol kg^{-1}, whereas maximum concentrations in the eastern basin only attain about 7 nmol kg^{-1}. It should be noted that most stations sampled in the western basin were located further south of those sampled in the eastern basin (see Figure 1).

[42] $[N_2O]_{xs}$ in waters deeper than 2000 m is at 1.9 ± 0.5 nmol kg^{-1} slightly elevated in the eastern basin compared to 1 ± 0.9 nmol kg^{-1} in the western basin. A paired *t*

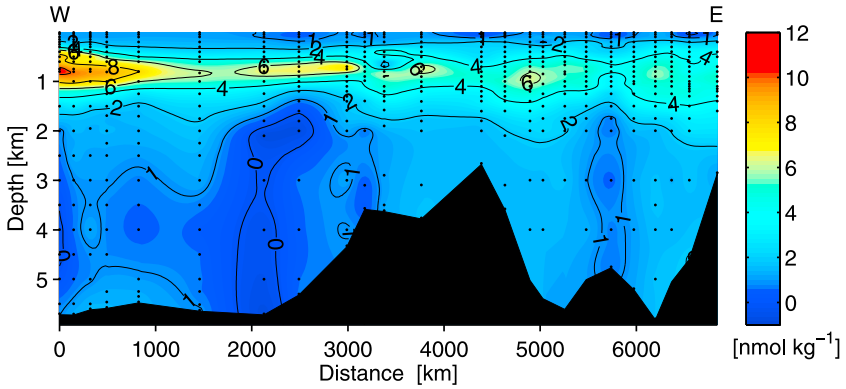

Figure 5. Section of excess N_2O (nmol kg^{-1}) calculated with the TTD method. For exact location of the section, see Figure 1.

test rejects the hypothesis that both samples originate from a distribution of equal mean and equal variance at the 1% significance level, but the overall level of excess N_2O accumulation in the deep water of either basin remains very low.

3.3. $[N_2O]_{xs}$/AOU Relationship

[43] Maximum $[N_2O]_{xs}$ coincides with maximum AOU concentrations. This indicates that the production of N_2O is due to nitrification consistent with the view of nitrification as the dominant production pathway of N_2O in the North Atlantic Ocean [*Walter et al.*, 2006; *Nevison et al.*, 2003; *Oudot et al.*, 2002; *Yoshinari*, 1976].

[44] The fact that $[N_2O]_{eq}$ is overestimated by 8–13% by the previously used "contemporary" approach implies that the earlier and widely reported correlations between apparent oxygen utilization (AOU) and $[N_2O]_{xs}$ are probably a distorted image of the true relationship between these quantities. While this distortion will not affect the interpretation of positive N_2O_{xs}/AOU correlations as qualitative indicators for the production of N_2O via nitrification, it may have an impact on the use of the quantitative characteristics of the relationship for the parameterization of N_2O in models [e.g., *Schmittner and Galbraith*, 2008; *Goldstein et al.*, 2003; *Suntharalingam and Sarmiento*, 2000].

[45] There are two different N_2O_{xs}/AOU relationship evident in our data. Therefore we have split the data into two parts: data points with potential densities <27.5 kg m^{-3} (<∼1000 m or "shallow") and data points with potential densities ≥27.5 kg m^{-3} (≥∼1000 m or "deep").

[46] Figure 6 presents these two least squares fits given by linear regression algorithms. The quantitative characteristics for all three approaches of $[N_2O]_{xs}$ are listed in Table 1. The "contemporary" approach significantly overestimates $[N_2O]_{eq}$ in middle-aged and older water masses by 8–13%. This results in a similar underestimation of $[N_2O]_{xs}$, whereas both methods, "contemporary" and "TTD" method, yield the same estimate of $[N_2O]_{xs}$ for mixed layer samples. This gives rise to the steeper slope in the fit calculated using the "TTD" approach compared to the fit to the "shallow" data calculated using the contemporary atmospheric N_2O concentration. The slope for the "contemporary" approach is 14% smaller than the slope for the "TTD" approach. For the "deep" data points, the slope for the "contemporary" approach is 1% larger than that for the "TTD" approach. The difference in the "deep" water results from the fact, that the "contemporary" method underestimates $[N_2O]_{xs}$ more strongly as the concerned water masses get older.

[47] The "layer" method does not account for mixing and thus slightly underestimates $[N_2O]_{eq}$ in old waters as it cannot reproduce the excess N_2O added to the respective water mass by mixing with younger waters enriched in N_2O. For intermediate waters, the atmospheric mixing ratio used for the calculations was equivalent to the atmospheric N_2O mixing ratio from 1970. Therefore, $[N_2O]_{eq}$ is underestimated for all water masses originating more recently than 1970, whereas it overestimates $[N_2O]_{eq}$ for older water masses in this depth range. For "shallow" samples the slope for the "layer" approach is 3% smaller than the slope for the "TTD" approach, indicating that most sampled intermediate water masses originated before 1970. For "deep" samples the slope for the "layer" approach is 7% smaller than the slope for the "TTD" approach. This implies that the age of intermediate water masses is underestimated, indicating that most sampled water masses between 1000 m and ∼1500 m originated before 1970.

3.4. N_2O Production Rates

[48] To quantify sources and sinks of N_2O, it is not sufficient to look at $[N_2O]_{xs}$ alone, but it is necessary to look at production rates. The $[N_2O]_{xs}$ distribution, on its own, is not useful in revealing sources of N_2O as the water mass age distribution in the ocean interior is highly variable. Production rates (N_2OPR; see section 2.6) can potentially shed more light on processes responsible for N_2O production.

[49] In order to check whether our TTD-based estimates of N_2OPR are reasonable, we first calculated AOU rates from the same data set. AOUR varies between 0.1 and 17 μmol kg^{-1} yr^{-1} (upper 500 m) and 0.1 and 13 μmol kg^{-1} yr^{-1} (500–1000 m), respectively. These rates agreed reasonably well with prior estimates of AOUR of 4–25 μmol kg^{-1} yr^{-1} (upper 500 m) and 1–10 μmol kg^{-1} yr^{-1} (500–1000 m), respectively, based on ^{3}H/^{3}He age determination for a similar region [*Jenkins and Wallace*, 1992]. The "TTD"

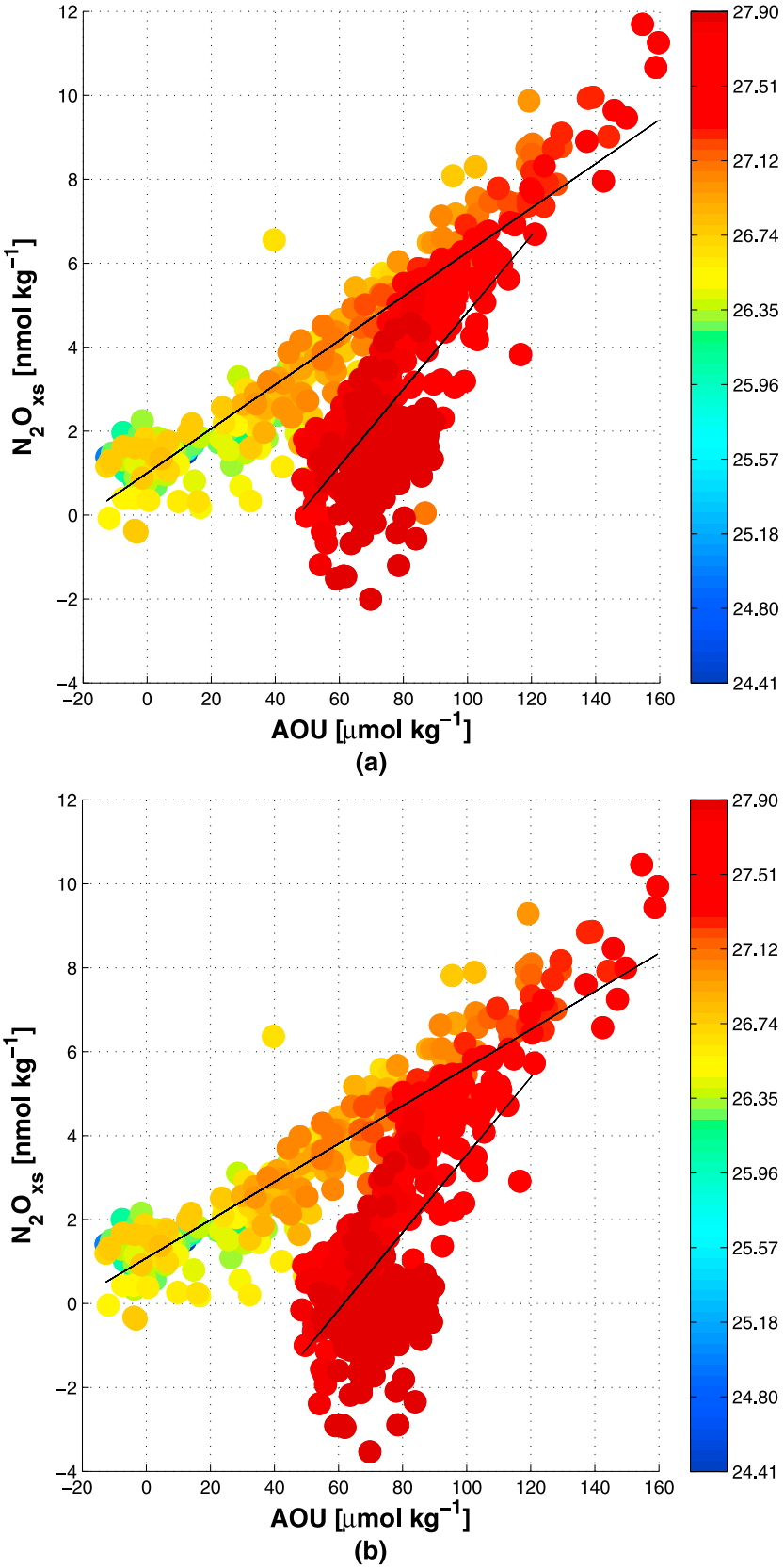

Figure 6. N_2O_{xs} concentrations (nmol kg^{-1}) versus AOU concentrations (μmol kg^{-1}); σ_θ is color coded in kg m^{-3}. (a) $[N_2O]_{xs}$ was calculated using the TTD method. (b) $[N_2O]_{xs}$ was calculated using only the contemporary mole fraction (319 ppb).

Table 1. Coefficients for a Least Squares Fit of $[N_2O]_{xs}$ Regressed on [AOU]

	TTD	Layer	Contemporary
Slope ($\sigma_\theta < 27.5$)	0.0526	0.0512	0.0454
Slope ($\sigma_\theta \geq 27.5$)	0.0916	0.0854	0.0924
Intercept ($\sigma_\theta < 27.5$)	1.0005	1.3271	1.0797
Intercept ($\sigma_\theta \geq 27.5$)	−4.3251	−3.7760	−5.7022

approach was also used by *Tanhua et al.* [2007] to estimate anthropogenic carbon concentrations and was found to be in good agreement with independent methods. This suggests that the use of CFC-12 and SF_6 as tracers is a good reliable basis for water mass age and hence rate calculations.

3.4.1. Influence of Depth and Remineralization

[50] Figure 7 shows N_2OPR plotted against depth. Maximum production rates occur just below the mixed layer, there is a lot of near-surface scatter, however. At most of the stations there is no subsurface maximum. Some stations between 30°N and 40°N in both basins display a small subsurface maximum, which mostly comprises just one sampled depth. The maximal production rate in the western basin of 1.9 nmol kg^{-1} yr^{-1} is only very slightly higher than the maximal production rate in the eastern basin of 1.7 nmol kg^{-1} yr^{-1}, and the general distribution is not significantly different, as is illustrated by the fitted curves displayed in red in Figure 7. Moreover, a paired t test does not reject the hypothesis that both samples originate from distributions with equal mean and equal variance at the 1% significance level.

[51] The black line in Figure 7 represents a Martin curve fitted to the data. Following *Martin et al.* [1987], this fitted curve $F(z)$ can be described as

$$F(z) = F_{100}\left(\frac{z}{100}\right)^{b}, \tag{10}$$

where F_{100} is the intercept of a log-log fit of the data, b is the slope of this log-log fit and z denotes depth.

[52] The parameters of the fit were determined using only the data from the eastern basin, but with the exception of the few very high rates, it fits the data from the western basin as well.

[53] Especially in waters deeper than 2000 m there seems to be very little variation, neither within or between basins. However, the dissolved oxygen concentrations in the eastern basin of 248 ± 5 μmol kg^{-1} are lower than the concentrations of 261 ± 7 μmol kg^{-1} in the western basin, probably due to the effects of the thermohaline circulation. A t test rejects the hypothesis that both oxygen samples originate from a distribution with equal mean and equal variance at the 1% significance level.

[54] Oceanic N_2O is mainly produced by nitrification and denitrification [*Bange*, 2008]. Since the waters of the North Atlantic are well oxygenated and denitrification only occurs in low-oxygen environments, a significant nitrous oxide source originating from denitrification processes seems very unlikely. Together with the fact that a Martin curve fits the data so well, this suggests that N_2O production in deep waters is controlled by the flux of organic particles from above as this flux is typically parameterized by a Martin curve. This seems reasonable as nitrification is fueled by organic particles, which are remineralized at depth.

3.4.2. Influence of AOU and Temperature

[55] As nitrification is supposed to be the main production mechanism, it is reasonable to quantify the N_2O yield per mole oxygen consumed ($\frac{dN_2O}{-dO_2}$). *Nevison et al.* [2003] argued, that $[N_2O]_{xs}$/AOU may not be an adequate estimate of $\frac{dN_2O}{-dO_2}$ due to the effects of mixing and advective transport. Mixing of water masses with different temperatures can create "virtual" supersaturations or undersaturations as the solubility function of N_2O depends nonlinearly on temperature. Following *Nevison et al.* [2003], we neglect this effect as it is probably small. We use N_2OPR/AOUR as an estimate of $\frac{dN_2O}{-dO_2}$. The influence of mixing on $[N_2O]_{eq}$ in terms of mixing of water with different ages is accounted for by the TTD approach (see section 2.5), which leaves the influence of mixing and advective transport on $[N_2O]_{xs}$ to be dealt with. It is important to note that our approach to estimation of $[N_2O]_{xs}$ integrates the effects of potentially varying production and decomposition mechanisms along the transport path of a water mass. Hence our N_2OPR and AOUR estimates represent smoothed and averaged quantities along the transport pathway. They provide average rates which are not necessarily representative of instantaneous or local rates.

[56] Figure 8 shows the ratio of N_2OPR to AOUR, both the ratios calculated from the M60/5 data and the ratios calculated according to the parameterization given by *Nevison et al.* [2003]. The latter parameterized $\frac{dN_2O}{-dO_2}$ as the N_2O yield of nitrification ($\frac{dN_2O}{-dNO_3^-}$) based on laboratory experiments by *Goreau et al.* [1980], i. e.

$$\frac{dN_2O}{-dO_2} = R_{N:O2}\ \frac{dN_2O}{-dNO_3^-}, \tag{11}$$

where $R_{N:O2}$ is the Redfield ratio. Noting the same exponential relationship we give in equation (13), the parameterization is extended to

$$\frac{dN_2O}{-dO_2} = R_{N:O2}\ \frac{dN_2O}{-dNO_3^-}\ \exp\left(-\frac{z}{z_{scale}}\right), \tag{12}$$

where z denotes depth and z_{scale} is a scaling factor.

[57] There seems to be a systematic difference between the two sets of ratios between 500 m and 1000 m. The parameterization of *Nevison et al.* [2003] displays a clear subsurface maximum in the production rates around 700 m. This is in general not reflected in our parameterization. There are, however, a few stations which display a subsurface maximum in the concerned depth range, which is obscured by the scatter in Figure 8. This discrepancy could be due to the fact that the results of *Goreau et al.* [1980] were obtained by studying a single nitrifying organism.

[58] The ratio of N_2OPR to AOUR depends exponentially on depth; that is, a relationship of the following type holds

$$\frac{N_2OPR}{AOUR} = a_1\ \exp\left(-\frac{z}{z_{sc}}\right), \tag{13}$$

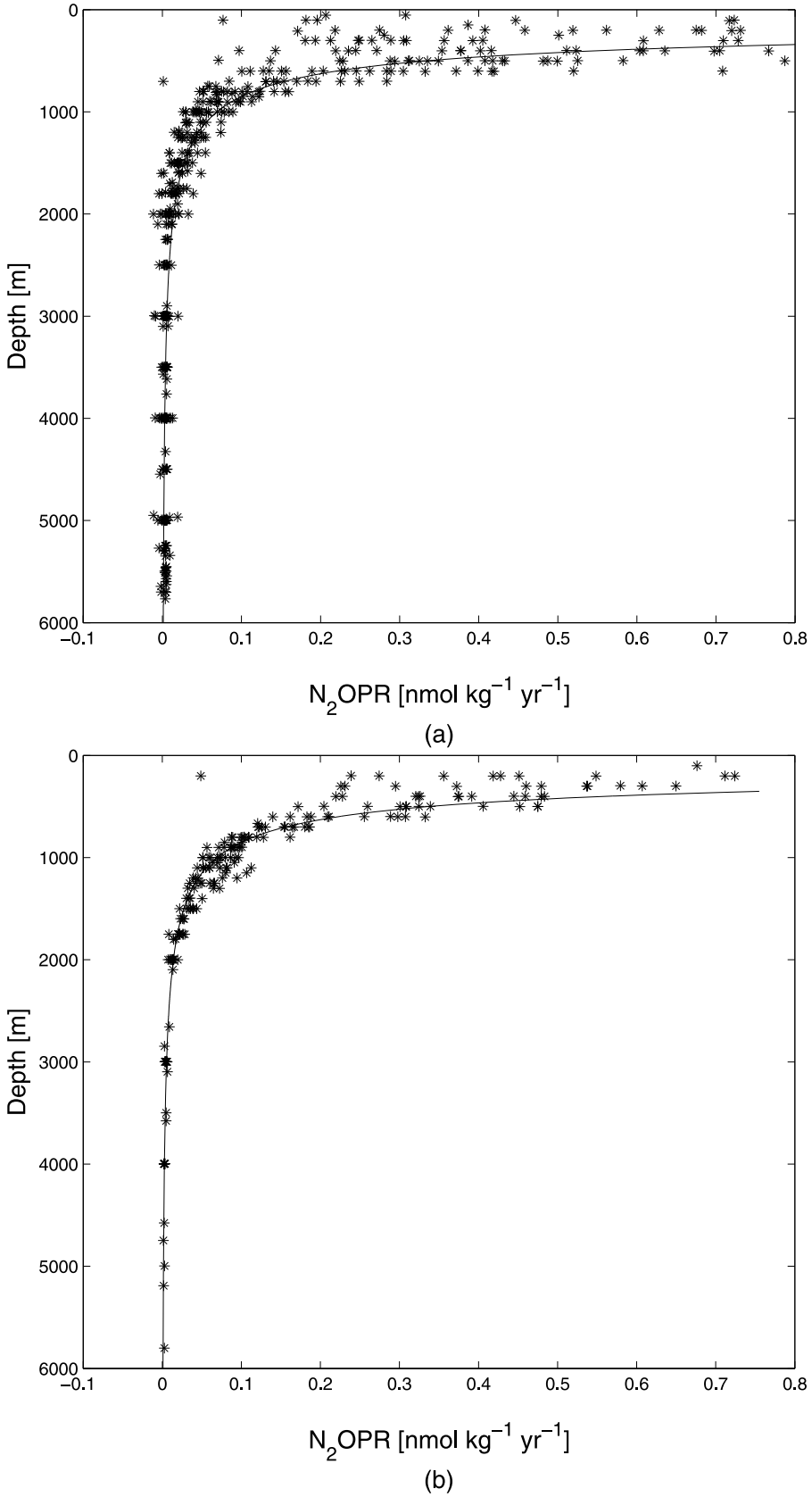

Figure 7. N_2O production rates (nmol kg^{-1} yr^{-1}) versus depth (m). The black lines show a Martin curve fitted to the respective data (see equation (10)). (a) Western basin of the North Atlantic Ocean. (b) Eastern basin of the North Atlantic Ocean.

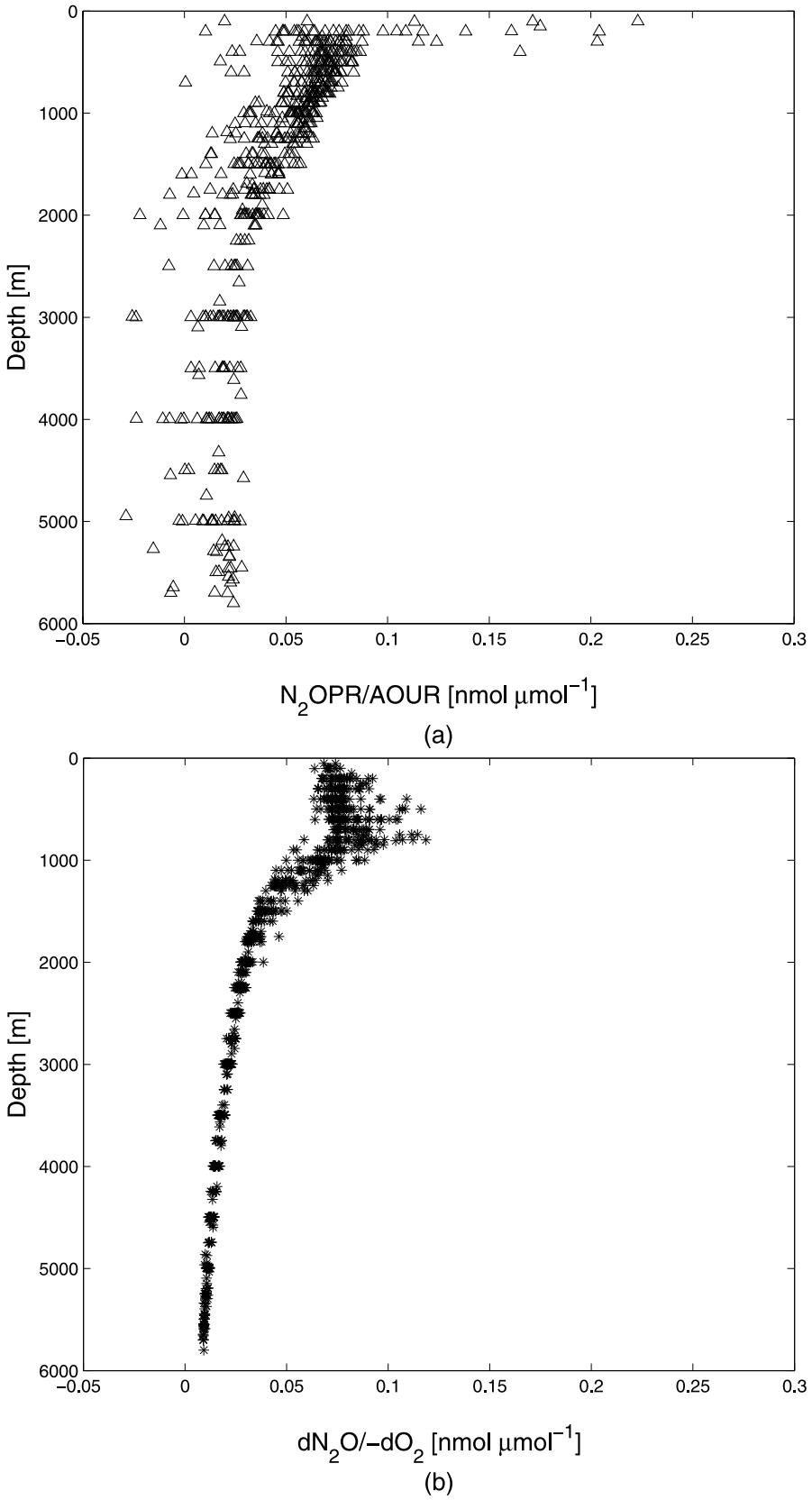

Figure 8. Comparison of $N_2OPR/AOUR$ and $\frac{dN_2O}{-dO_2}$. (a) $N_2OPR/AOUR$ (nmol μmol^{-1}) versus depth (m), with ratios calculated from the M60/5 data; (b) $\frac{dN_2O}{-dO_2}$ calculated using the parameterization given by *Nevison et al.* [2003].

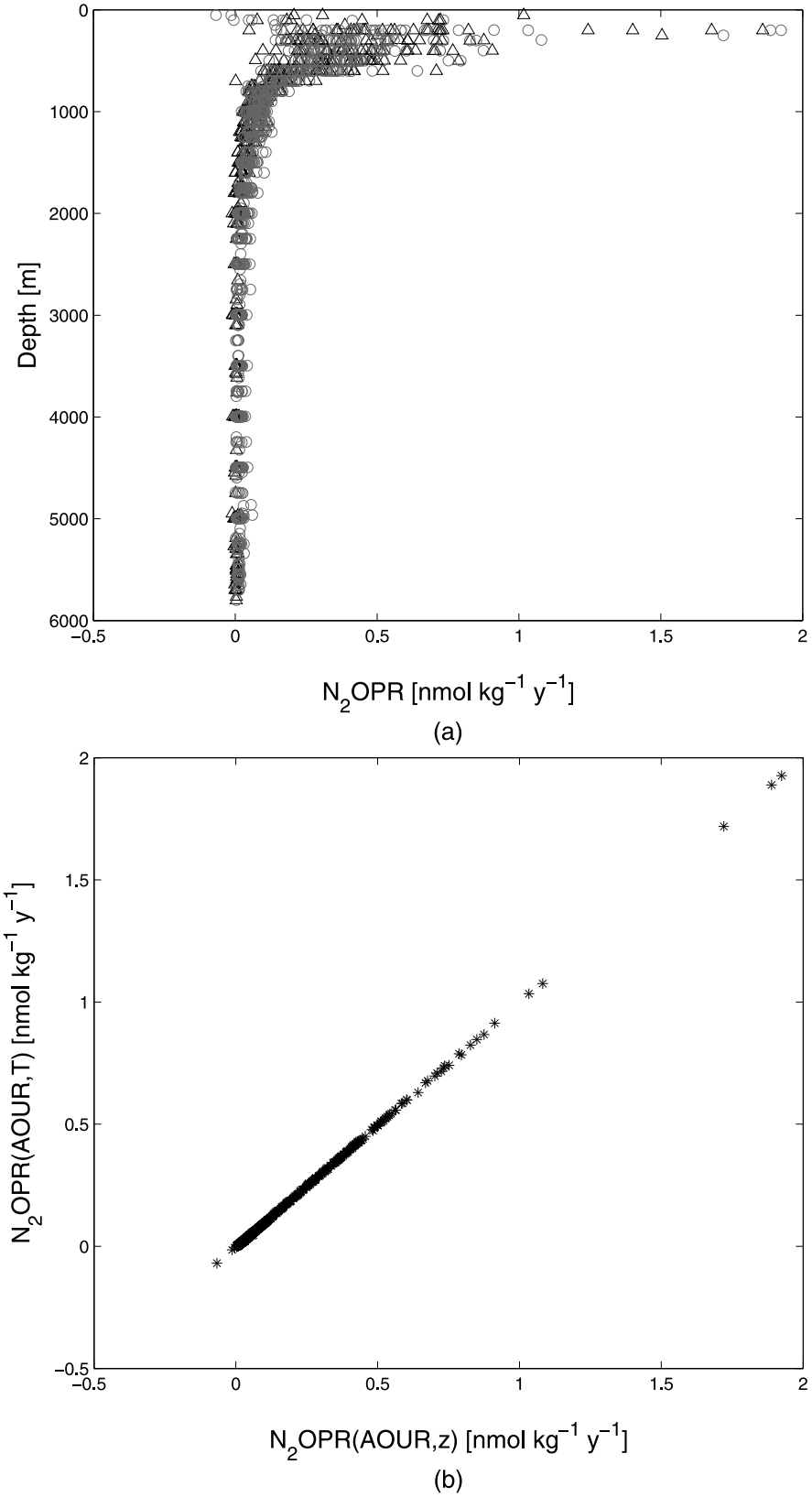

Figure 9. Comparison of N_2OPR calculated from in situ data and fitted values. (a) N_2OPR (nmol kg^{-1} yr^{-1}) versus depth (m). Black triangles denote the N_2O production rates calculated from the M60/5 data, and gray circles denote the fitted values given by equation (14). (b) Fitted values of N_2OPR according to equation (15) versus fitted values of N_2OPR according to equation (14).

where a_1 and z_{sc} are scaling factor and z denotes the depth. This seems to suggest that with greater depth the by-path in nitrification that produces N_2O is less frequently used. This might be related to the general decline in temperature with depth or the decrease in the overall nitrification rate with depth. With the present data it is impossible to assign a reason for this trend, which could also be an effect of a change in community structure.

[59] We used this relationship to develop a parameterization of N_2OPR against AOUR and depth. Using equation (13), the best fit to our data can be described as

$$N_2OPR(AOUR, z) = AOUR\ a_1\ \exp\left(-\frac{z}{z_{sc}}\right) + a_2, \qquad (14)$$

where the coefficient values for the best fit are $a_1 = 0.0658$, $a_2 = -0.0065$, $z_{sc} = 20000$ and z denotes the depth.

[60] As depth is strongly correlated with temperature and the latter may have a stronger biological influence it seems reasonable to also develop a parameterization of N_2OPR based on temperature instead of depth. Equation (14) then translates into:

$$N_2OPR(AOUR, T) = AOUR\ a_1\ \exp\left(-\frac{T}{T_{sc}}\right) + a_2, \qquad (15)$$

where the coefficient values for the best fit are $a_1 = 0.0665$, $a_2 = -0.0032$, $T_{sc} = 20000$ and T denotes the temperature.

[61] Figure 9 shows the N_2O production rates calculated from the M60/5 data. The fitted values according to equation (14), and the correlation between the fits given by equations (14) and (15), respectively, illustrate the goodness of our fits (Figure 9). Our parameterizations only account for N_2O production by nitrification. However, due to lack of oxygen the AOURs in anoxic zones will be very small. Therefore this parameterization also effectively reproduces the decreasing to vanishing N_2O production due to nitrification in suboxic to anoxic zones, which a parameterization simply based on AOU is incapable of doing. Therefore this parameterization can be used to calculate N_2O production due to nitrification without having to introduce a somewhat artificial critical oxygen threshold. Our parameterizations can be used to calculate global N_2O concentration fields with any coupled GCM/biogeochemical model, which allows for apparent oxygen utilization rates to be calculated. Additionally, these parameterizations facilitate the calculation of global $[N_2O]$ fields using existing gridded tracer [*Key et al.*, 2004] and AOU data [*Garcia et al.*, 2006].

4. Conclusions

[62] 1. The commonly employed method of using just the contemporary atmospheric mixing ratio of N_2O to calculate $[N_2O]_{xs}$ underestimates the strength of possible N_2O sources. Due to this, the quantitative characteristics of the widely used correlation between AOU and $[N_2O]_{xs}$ are biased. Especially as the quantitative characteristics of this relationship form the basis for calculation of N_2O production rates, it is of importance to estimate this relationship as accurately as possible. The TTD approach introduced here provides a way to calculate appropriately "age-corrected" excess N_2O concentrations. The difference in slopes of the correlation between AOU and $[N_2O]_{xs}$ is up to 14% for the "contemporary" versus the "TTD" approach and up to 7% for the "layer" versus the "TTD" approach.

[63] 2. $N_2O_{xs}^{TTD}$ concentrations found in the North Atlantic are similar to those found in previous studies. Largest concentrations of N_2O_{xs} are found between 700 m and 1000 m. This accumulation of N_2O_{xs} reflects a balance between production and water mass age.

[64] 3. We used TTDs to calculate AOUR and N_2OPR. AOURs are similar to the rates found in earlier studies. N_2OPR correlates well with AOUR and correlates inversely with depth and/or temperature.

[65] 4. We developed a new parameterization of N_2OPR in terms of AOUR and temperature and depth, which can be used in biogeochemical models and to calculate $N_2OPR/[N_2O]$ from existing global gridded data like GLODAP/WOA. It differs from earlier parameterizations, as it parameterizes a N_2O production rate per time step in terms of an oxygen utilization rate per time step instead of a N_2O production rate per mole oxygen consumed. Our parameterization can be applied to calculate the N_2O production due to nitrification in the entire ocean including oxygen minimum zones, as AOUR, in contrast to AOU, tends to become very small at very low oxygen levels.

[66] **Acknowledgments.** This study was supported by the German Science Foundation (DFG) by research grants DFG BA 1990/7 and DFG WA 1434/5 and BMBF grant 03F0462A. We would like to thank two anonymous reviewers for their valuable comments.

References

Bange, H. W. (2008), Gaseous nitrogen compounds (NO, N_2O, N_2, NH_3) in the ocean, in *Nitrogen in the Marine Environment*, 2nd ed., edited by D. G. Capone et al., pp. 51–94, Elsevier, New York.

Battle, M., et al. (1996), Atmospheric gas concentrations over the past century measured in air from firn at the South Pole, *Nature*, *383*, 231–235.

Broecker, W. S., and T.-H. Peng (2000), Comparison of ^{39}Ar and ^{14}C ages for waters in the deep ocean, *Nuclear Instr. Methods Phys. Res. B*, *172*, 473–478.

Bullister, J., and R. Weiss (1988), Determination of CCl_3F and CCl_2F_2 in seawater and air, *Deep Sea Res., Part A*, *35*(5), 839–853.

Bullister, J., D. Wisegarver, and F. Menzia (2002), The solubility of sulfur hexafluoride in water and seawater, *Deep Sea Res., Part I*, *49*(1), 175–187.

Butler, J. H., J. W. Elkins, and T. M. Thompson (1989), Tropospheric and dissolved N_2O of the west Pacific and east Indian oceans during the El Niño southern oscillation event of 1987, *J. Geophys. Res.*, *94*(D12), 14,865–14,887.

Flückinger, J., A. Dallenbach, T. Blunier, B. Stauffer, T. F. Stocker, D. Raynaud, and J. M. Barnola (1999), Variations in atmospheric N_2O concentrations during abrupt climatic changes, *Science*, *285*, 227–230.

Garcia, H. E., R. A. Locarnini, T. P. Boyer, and J. I. Antonov (2006), *World Ocean Atlas 2005, vol. 3, Dissolved Oxygen, Apparent Oxygen Utilization and Oxygen Saturation, NOAA Atlas NESDIS 63*, edited by S. Levitus, 342 pp., U.S. Govt. Print. Off., Washington, D. C.

Goldstein, B., F. Joos, and T. F. Stocker (2003), A modeling study of oceanic nitrous oxide during the Younger Dryas cold period, *Geophys. Res. Lett.*, *30*(2), 1092, doi:10.1029/2002GL016418.

Goreau, T. J., W. A. Kaplan, S. C. Wofsy, M. B. McElroy, F. W. Valois, and S. W. Watson (1980), Production of NO_2^- and N_2O by nitrifying bacteria at reduced concentrations of oxygen, *Appl. Environ. Microbiol.*, *40*(3), 526–532.

Holland, E. A., J. Lee-Taylor, C. Nevison, and J. Sulzman (2005), Fluxes and N_2O mixing ratios originating from human activity, data set, DAAC, Oak Ridge Natl. Lab., Oak Ridge, Tenn. (Available at http://daac.ornl.gov/)

IPCC (2007), *Climate Change 2007: Synthesis Report. Contribution of Working Groups I, II and III to the Fourth Assessment Report of the Intergovernmental Panel on Climate Change*, 104 pp., IPCC, Geneva.

Jenkins, W. J., and D. W. R. Wallace (1992), Tracer-based inferences of new primary production in the sea, in *Primary Productivity and Biogeochemical Cycles in the Sea*, edited by P. G. Falkowski and A. D. Woodhead, pp. 299–316, Plenum Press, New York.

Key, R. M., et al. (2004), A global ocean carbon climatology: Results from Global Data Analysis Project (GLODAP), *Global Biogeochem. Cycles*, *18*, GB4031, doi:10.1029/2004GB002247.

Körtzinger, A., J. Schimanski, U. Send, and D. W. R. Wallace (2004), The ocean takes a deep breath, *Science*, *306*, 1337.

Machida, T., T. Nakazawa, Y. Fujii, S. Aoki, and O. Watanabe (1995), Increase in the atmospheric nitrous oxide concentration during the last 250 years, *Geophys. Res. Lett.*, *22*(21), 2921–2924.

Maiss, M., and C. Brenninkmeijer (1998), Atmospheric SF6: Trends, sources, and prospects, *Environ. Sci. Technol.*, *232*(20), 3077–3086.

Martin, J. H., G. A. Knauer, D. M. Karl, and W. W. Broenkow (1987), VERTEX: Carbon cycling in the northeast Pacific, *Deep Sea Res., Part A*, *34*(2), 267–285.

Najjar, R. G. (1992), Marine biogeochemistry, in *Climate System Modeling*, edited by K. E. Trenberth, pp. 241–280, Cambridge Univ. Press, Cambridge, UK.

Nevison, C., R. F. Weiss, and D. J. Erickson III (1995), Global oceanic emissions of nitrous oxide, *J. Geophys. Res.*, *100*(C8), 809–815.

Nevison, C., J. H. Butler, and J. W. Elkins (2003), Global distribution of N_2O and the ΔN_2O-AOU yield in the subsurface ocean, *Global Biogeochem. Cycles*, *17*(4), 1119, doi:10.1029/2003GB002068.

Oudot, C., P. Jean-Baptiste, E. Fourré, C. Mormiche, M. Guevel, J.-F. o. Ternon, and P. Le Corre (2002), Transatlantic equatorial distribution of nitrous oxide and methane, *Deep Sea Res., Part I*, *49*(7), 1175–1193.

Prinn, R., et al. (2000), A history of chemically and radiatively important gases in air deduced from ALE/GAGE/AGAGE, *J. Geophys. Res.*, *105*(D14), 17,751–17,792.

Schmittner, A., and E. D. Galbraith (2008), Glacial greenhouse-gas fluctuations controlled by ocean circulation changes, *Nature*, *456*(7220), 373–376.

Suntharalingam, P., and J. Sarmiento (2000), Factors governing the oceanic nitrous oxide distribution: Simulations with an ocean general circulation model, *Global Biogeochem. Cycles*, *14*(1), 429–454.

Tanhua, T., K. Bulsiewicz, and M. Rhein (2005), Spreading of overflow water from the Greenland to the Labrador Sea, *Geophys. Res. Lett.*, *32*, L10605, doi:10.1029/2005GL022700.

Tanhua, T., A. Biastoch, A. Körtzinger, H. Lüger, C. Böning, and D. Wallace (2006), Changes of anthropogenic CO_2 and CFCs in the North Atlantic between 1981 and 2004, *Global Biogeochem. Cycles*, *20*, GB4017, doi:10.1029/2006GB002695.

Tanhua, T., A. Körtzinger, K. Friis, D. Waugh, and D. Wallace (2007), An estimate of anthropogenic CO2 inventory from decadal changes in oceanic carbon content, *Proc. Natl. Acad. Sci. U. S. A.*, *104*(9), 3037–3042, doi:10.1073/pnas.0606574104.

Tanhua, T., D. Waugh, and D. Wallace (2008), Use of SF6 to estimate anthropogenic CO_2 in the upper ocean, *J. Geophys. Res.*, *113*, C04037, doi:10.1029/2007JC004416.

Walker, S., R. Weiss, and P. Salameh (2000), Reconstructed histories of the annual mean atmospheric mole fractions for the halocarbons CFC-11, CFC-12, CFC-113, and carbon tetrachloride, *J. Geophys. Res.*, *105*(C6), 14,285–14,296.

Walter, S., H. W. Bange, U. Breitenbach, and D. W. R. Wallace (2006), Nitrous oxide in the North Atlantic Ocean, *Biogeosciences*, *3*(4), 607–619.

Warner, M. J., and R. F. Weiss (1985), Solubilities of chlorofluorocarbons 11 and 12 in water and sea water, *Deep Sea Res., Part I*, *32*(12), 1485–1497.

Waugh, D. W., T. M. Hall, and T. W. N. Haine (2003), Relationships among tracer ages, *J. Geophys. Res.*, *108*(C5), 3138, doi:10.1029/2002JC001325.

Waugh, D. W., T. M. Hall, and T. W. N. Haine (2004), Transport times and anthropogenic carbon in the subpolar North Atlantic Ocean, *Deep Sea Res., Part I*, *51*(11), 1475–1491.

Weiss, R., and B. Price (1980), Nitrous oxide solubility in water and seawater, *Mar. Chem.*, *8*(4), 347–359.

Yoshinari, T. (1976), Nitrous oxide in the sea, *Mar. Chem.*, *4*, 189–202.

H. W. Bange, A. Freing, T. Tanhua, and D. W. R. Wallace, Marine Biogeochemistry Research Division, Leibniz Institute for Marine Sciences, IFM-GEOMAR, Düsternbrooker Weg 20, Kiel D-24105, Germany. (afreing@ifm-geomar.de)

S. Walter, IMAU, Utrecht University, PO Box 80005, NL-3508 TA Utrecht, Netherlands.